Anomalous Diffusion in the Long-Range Haken-Strobl-Reineker Model

A. G. Catalano,[1,2] F. Mattiotti,[1] J. Dubail,[1,3] D. Hagenmüller,[1] T. Prosen,[4] F. Franchini,[2] and G. Pupillo[1,5]
[1]University of Strasbourg and CNRS, CESQ and ISIS (UMR 7006), aQCess, 67000 Strasbourg, France
[2]Institut Ruđer Bošković, Bijenička cesta 54, 10000 Zagreb, Croatia
[3]Université de Lorraine and CNRS, LPCT (UMR 7019), 54000 Nancy, France
[4]Faculty for Mathematics and Physics, University of Ljubljana, Jadranska ulica 19, 1000 Ljubljana, Slovenia
[5]Institut Universitaire de France (IUF), 75000 Paris, France

(Received 15 December 2022; accepted 17 July 2023; published 3 August 2023)

We analyze the propagation of excitons in a d-dimensional lattice with power-law hopping $\propto 1/r^{\alpha}$ in the presence of dephasing, described by a generalized Haken-Strobl-Reineker model. We show that in the strong dephasing (quantum Zeno) regime the dynamics is described by a classical master equation for an exclusion process with long jumps. In this limit, we analytically compute the spatial distribution, whose shape changes at a critical value of the decay exponent $\alpha_{\mathrm{cr}} = (d+2)/2$. The exciton always diffuses anomalously: a superdiffusive motion is associated to a Lévy stable distribution with long-range algebraic tails for $\alpha \leq \alpha_{\mathrm{cr}}$, while for $\alpha > \alpha_{\mathrm{cr}}$ the distribution corresponds to a surprising mixed Gaussian profile with long-range algebraic tails, leading to the coexistence of short-range diffusion and long-range Lévy flights. In the many-exciton case, we demonstrate that, starting from a domain-wall exciton profile, algebraic tails appear in the distributions for any α, which affects thermalization: the longer the hopping range, the faster equilibrium is reached. Our results are directly relevant to experiments with cold trapped ions, Rydberg atoms, and supramolecular dye aggregates. They provide a way to realize an exclusion process with long jumps experimentally.

DOI: 10.1103/PhysRevLett.131.053401

Introduction.—Energy transport is of fundamental importance in biological, chemical, and physical systems. In light-harvesting setups, for example, solar energy is converted into excitons that are transported to a reaction center or to the interface between two different semiconductors, which often relies on long-range dipolar couplings between the excitons [1–3]. Transport then results from a competition between coherent hopping that tends to delocalize the wave functions and local couplings to vibrational, motional degrees of freedom and disorder potentials, which lead to the localization of carriers [4–7], limiting the conversion efficiency of optoelectronic devices [8]. Theory has mostly focused on short-range couplings among quantum emitters, as they allow simple analytical approaches. For instance, the interplay between short-range hopping and local dephasing, which can be induced by, e.g., thermal noise or vibrational coupling [9], is captured by the Haken–Strobl–Reineker (HSR) model: for large enough dephasing, a transition from ballistic to diffusive motion occurs at time $t \sim 1/\gamma$ [10–12], with γ the local dephasing rate. Diffusion taking place for $t \gg 1/\gamma$ is standard, i.e., an initially localized exciton spreads as a Gaussian distribution $\exp(-r^2/4Dt)$, with a diffusion coefficient $D = 2J^2/\gamma$ (J is the nearest-neighbor hopping rate). While the HSR model with nearest-neighbor hopping has been extensively analyzed and even solved exactly [10–14], the interplay of power-law long-range hopping and dephasing is more challenging and has not been analytically treated. Power-law hopping stems from the $\sim 1/r^3$ dipolar coupling in molecular aggregates [1–3] or nanocrystals [15–17], for instance, where large dephasing is naturally present [18–21]. More general power-law-type couplings with arbitrary spatial decay can be engineered in artificial systems such as cold trapped ions [22,23] or Rydberg gases [24–26].

In this Letter, we investigate the HSR model with coupling between quantum emitters that decays with distance r as a power law $\sim 1/r^{\alpha}$, with variable power α and for a generic dimension d. In the presence of strong dephasing—in the quantum Zeno regime [27]—we map the system to a classical master equation (CME) that captures the long-time dynamics $t \gg 1/\gamma$, which we solve exactly by analytical and numerical means.

We find that excitons always diffuse anomalously: in the single-exciton limit, the CME is the one of a discrete random walk with long jumps, or discrete Lévy flight [28–30], and for any finite α the exciton density profile always decays algebraically at long distances, in contrast to the standard diffusion obtained from the HSR model with nearest-neighbor hopping. The interaction range α determines whether the variance of the distribution converges or not: based on this, we define the critical exponent $\alpha_{\mathrm{cr}} = (d+2)/2$. For $\alpha \leq \alpha_{\mathrm{cr}}$, the dynamics is superdiffusive and the exciton density at sufficiently long

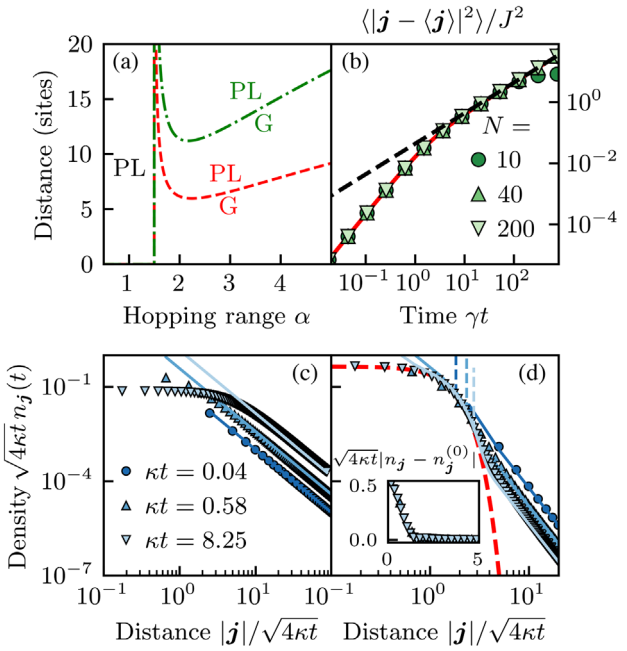

FIG. 1. Single-exciton regime for $d = 1$: time evolution of an exciton initially located at site $\mathbf{0}$. The exciton density profile $n_j(t)$ is characterized by a power law (PL) at long distance and a Gaussian (G) at short distance (a). The boundary between the two regions (red dashed line for $\kappa t = 1$ and green dashed-dotted line for $\kappa t = 3$) corresponds to $\xi_{\alpha,t}$ [see Eq. (10)]. The quantum to classical crossover is illustrated through the time evolution of the exciton variance (b), obtained by numerically solving Eq. (1) for $\alpha = 3$ and $\gamma = 10J$. Red solid line, exact solution Eq. (3); black dashed line, classical approximation for $\gamma t \gg 1$ [Eq. (4)]. A pure power-law density profile for $\alpha = 1 < \alpha_{\rm cr}$ (c) and mixed Gaussian power law for $\alpha = 2 > \alpha_{\rm cr}$ (d) are obtained by numerically solving Eq. (7) for $N = 1000$ and $\gamma = 10J$. Solid lines, approximation Eq. (10); thick red dashed line, Gaussian term in Eq. (10b); thin dashed lines, $\xi_{\alpha,t}$. The diffusion enhancement with respect to the case $\alpha \to \infty$ $[n_j^{(0)}(t)]$ is shown in the inset.

distance is always a Lévy stable distribution [29–32] characterized by a long-range algebraic tail $\sim 1/r^{2\alpha}$. For $\alpha > \alpha_{\rm cr}$ and small enough time, the exciton density is also solely characterized by an algebraic tail, while at long time it exhibits a surprising mixed profile corresponding to a Gaussian distribution at short distance and an algebraic tail at large distance [Fig. 1(a)]. The Gaussian part of the distribution mimics the standard diffusion in the HSR model. However, remarkably, also this Gaussian contribution is nonstandard as the diffusion coefficient depends on α and is enhanced by the long-range character of the hopping. We show that this finding is relevant to long-range exciton diffusion in light-harvesting systems such as nanocrystal quantum dots, where discrepancies between experimental observations and theory have been reported.

We find that in the case of many excitons our model is equivalent to a long-jump symmetric exclusion process [33–35], with a Markov matrix identical to the Hamiltonian of a long-range ferromagnetic Heisenberg model. Long-range hopping enhances exciton propagation so that equilibrium is reached faster as α is decreased. We capture the equilibration dynamics analytically via a continuous diffusion equation with fractional Laplacian that qualitatively reproduces the numerical results for all α.

Excitons are modeled as spin-1/2 operators S. We start with the single-exciton case and study the dynamics in the presence of dephasing governed by the HSR quantum master equation

$$\dot{\rho} = -i[H,\rho] + \gamma \sum_j \left(L_j \rho L_j^\dagger - \frac{1}{2}\{L_j^\dagger L_j, \rho\} \right) = \hat{\mathcal{L}}\rho. \tag{1}$$

In our case, the coherent dynamics is described by the power-law hopping Hamiltonian

$$H = \frac{1}{2}\sum_j \sum_{\boldsymbol{r}\neq\mathbf{0}} \frac{J}{r^\alpha}(S_j^+ S_{j+\boldsymbol{r}}^- + S_j^- S_{j+\boldsymbol{r}}^+), \tag{2}$$

with ρ the density matrix, $\boldsymbol{j} \in \mathbb{Z}^d$ the position in a d-dimensional lattice, $r = |\boldsymbol{r}|$, and $L_j = L_j^\dagger = S_j^z$ the local dephasing operators, in the Lindblad formalism [36,37]. For $d = 1$ and when a single exciton is initially present on a given site, it is known that the variance of the exciton evolves in time as [10]

$$\langle|\boldsymbol{j}-\langle\boldsymbol{j}\rangle|^2\rangle = 2\sum_{\boldsymbol{r}} \frac{r^2 H_{\boldsymbol{r}}^2}{\gamma^2}(\gamma t + e^{-\gamma t} - 1), \tag{3}$$

with $H_{\boldsymbol{r}} = \langle G|S_j^- H S_{j+\boldsymbol{r}}^+|G\rangle$ and $|G\rangle$ the ground state with all the spins down. The short- and long-time approximations of Eq. (3) read

$$\langle|\boldsymbol{j}-\langle\boldsymbol{j}\rangle|^2\rangle \approx \begin{cases} \sum_{\boldsymbol{r}} r^2 H_{\boldsymbol{r}}^2 t^2 & \text{for } \gamma t \ll 1 \\ 2\sum_{\boldsymbol{r}} \frac{r^2 H_{\boldsymbol{r}}^2}{\gamma} t & \text{for } \gamma t \gg 1, \end{cases} \tag{4}$$

and reveal a crossover in the dynamics: while a coherent quantum dynamics dominates for a short time, a classical diffusivelike behavior emerges for $t \gg 1/\gamma$. This is illustrated in Fig. 1(b), where the exciton variance is obtained by numerically solving the quantum master Eq. (1) for different system sizes N, and compared to the analytical solutions Eqs. (3) and (4). The crossover from ballistic to diffusive regime is clearly visible. Interestingly, the transition to the classical regime always occurs at $t \sim 1/\gamma$, independently of N and α [38]. This is because in Eq. (4), the same multiplicative factor $\sum_{\boldsymbol{r}} r^2 H_{\boldsymbol{r}}^2$ governs both the short- and late-time behaviors, so the crossover timescale is independent of the details of the Hamiltonian. In Fig. 1(b) we see that for $\gamma t \gtrsim 10$, the quantum dissipative evolution is indistinguishable from the long-time asymptotics in Eq. (4).

Importantly, Eq. (3) implies that the late-time diffusive-like regime is always reached, for any dephasing strength γ. This can also be seen from the quantum master Eq. (1). Indeed, for any dephasing, we observe numerically that for large system size and long time ($t \gg 1/\gamma$) the coherences in the single-particle density matrix, $G_{j,m} = \mathrm{Tr}[\rho S_j^+ S_m^-]$, with $j \neq m$, become negligible with respect to the population density $n_j = G_{j,j}$. However, in the limit of weak dephasing, this effect cannot simply be explained from perturbation theory in γ, as the long-time dynamics is determined by a nonperturbative branch of eigenmodes of the Liouvillian $\hat{\mathcal{L}}$ [Eq. (1)] [38]. An analogous effect has been observed in the case of nearest-neighbor hopping with dephasing and more sophisticated techniques should be used [14]. We leave this for future work. Next we turn to the strong dephasing limit, which can be handled analytically more easily.

Strong dephasing: Mapping to classical Markov process.—Following Refs. [42,43], we use a second-order perturbative analysis, deriving an effective Liouvillian $\hat{\mathcal{L}}_{\mathrm{eff}}$ in the limit $\gamma \gg J$ (for similar treatments of the strong dissipative limit, see also [44,45] for soft-core bosons and nearest-neighbor hopping, or [46,47] for atom losses instead of dephasing). We split the Liouvillian Eq. (1) into two contributions: a term $\hat{\mathcal{L}}_0\rho = \gamma \sum_j (S_j^z \rho S_j^z - \rho/4)$, and a perturbation $\hat{\mathcal{L}}_1\rho = -i[H,\rho]$. We find [38] that the effective dynamics $\dot{\rho} = \mathcal{L}_{\mathrm{eff}}\rho$ is governed by a CME for the probability distribution

$$\dot{p}(\boldsymbol{\sigma}) = -\sum_{\boldsymbol{\sigma}'} \langle \boldsymbol{\sigma}|R|\boldsymbol{\sigma}'\rangle p(\boldsymbol{\sigma}'), \tag{5}$$

with $|\boldsymbol{\sigma}\rangle$ the eigenstates of the S_j^z operators, and $p(\boldsymbol{\sigma})$ the probability distribution defined by the diagonal entries of the density matrix $\rho = \sum_{\boldsymbol{\sigma}} p(\boldsymbol{\sigma})|\boldsymbol{\sigma}\rangle\langle\boldsymbol{\sigma}|$. The generator of the CME [Eq. (5)] is that of an exclusion process with long jumps, which turns out to be identical to the following Hamiltonian of a long-range ferromagnetic Heisenberg model:

$$R = -\sum_{j;r\neq 0} \frac{2J^2}{\gamma r^{2\alpha}} \left[\frac{1}{2}(S_j^+ S_{j+r}^- + S_j^- S_{j+r}^+) + S_j^z S_{j+r}^z - \frac{1}{4}\right]. \tag{6}$$

A similar observation was made in Refs. [42,43] for strictly short-range models, whose strong-dephasing limit corresponds to a ferromagnetic Heisenberg model with short-range couplings; here, we extend this result to long-range hopping. We note that, interestingly, the case $\alpha = d = 1$ in Eq. (6) corresponds to the Haldane-Shastry Hamiltonian [48], a famous quantum integrable model. For any exciton number, the associated exclusion process should then be exactly solvable by Bethe ansatz techniques, which we will investigate in a future work.

Anomalous diffusion of single exciton.—We first focus on the classical dynamics dictated by Eq. (5) for the case of a single exciton. Equation (6) provides the evolution of the population density

$$\dot{n}_j = \sum_{r\neq 0} \frac{\kappa}{r^{2\alpha}} (n_{j+r} - n_j), \tag{7}$$

with the effective Zeno-like rate $\kappa = 2J^2/\gamma$. An alternative derivation of Eq. (7) is obtained by adiabatically eliminating the coherences of the single-exciton density matrix $G_{j,m}$ [10,27,38]. Notice that Eq. (7) is well defined in the thermodynamic limit only if $\alpha > d/2$ so that $\sum_{r\neq 0} r^{-2\alpha}$ is finite. In order to solve Eq. (7) for an exciton initially at the origin, $n_j(t=0) = \delta_{j,0}$, we introduce the characteristic function $K(\boldsymbol{q},t) = \sum_j n_j(t) e^{i\boldsymbol{q}\cdot\boldsymbol{j}}$, where $\boldsymbol{q} \in \mathbb{R}^d$. Using Eq. (7), we find that the characteristic function at time t then reads

$$K(\boldsymbol{q},t) = e^{[\mathcal{A}_{2\alpha,d}(\boldsymbol{q}) - \mathcal{A}_{2\alpha,d}(\boldsymbol{0})]t}, \tag{8}$$

with the initial condition $K(\boldsymbol{q},0) = 1$, and $\mathcal{A}_{2\alpha,d}(\boldsymbol{q}) = \kappa \sum_{r\neq 0} r^{-2\alpha} e^{-i\boldsymbol{q}\cdot\boldsymbol{r}}$. Equation (8) provides the time evolution of the mean position $\langle \boldsymbol{j} \rangle = -i\nabla_{\boldsymbol{q}} K(\boldsymbol{0},t) = \boldsymbol{0}$ and of the variance $\langle |\boldsymbol{j}|^2 \rangle = -\Delta_{\boldsymbol{q}} K(\boldsymbol{0},t) = 2D_\alpha t$. The diffusion coefficient $D_\alpha = \frac{1}{2}\mathcal{A}_{2\alpha-2,d}(\boldsymbol{0})$ provides a first insight into the character of the dynamics for different α (however, see also discussion below): diffusivelike spreading of excitons takes place when D_α converges in the thermodynamic limit, which is ensured when $\alpha > \alpha_{\mathrm{cr}}$ [38]. This corresponds to the quantum master equation solution in the regime $\gamma t \gg 1$, shown in Eq. (4) and Fig. 1(b). On the other hand, for $\alpha \leq \alpha_{\mathrm{cr}}$, D_α diverges and the dynamics is superdiffusive. Equation (8) further allows one to determine the exciton density profile $n_j(t)$ for all α and times t. Since the long-distance behavior of $n_j(t)$ is determined by the singularity of $K(\boldsymbol{q},t)$ when $q \equiv |\boldsymbol{q}| \to 0$, we analyze $\mathcal{A}_{2\alpha,d}(\boldsymbol{q})$ in that limit. We find $\mathcal{A}_{2\alpha,d}(\boldsymbol{q}) \approx \mathcal{A}_{2\alpha,d}(\boldsymbol{0}) - C_\alpha q^{2\alpha-d}$ if $\alpha \leq \alpha_{\mathrm{cr}}$, and $\mathcal{A}_{2\alpha,d}(\boldsymbol{q}) \approx \mathcal{A}_{2\alpha,d}(\boldsymbol{0}) - [\mathcal{A}_{2\alpha-2,d}(\boldsymbol{0})/2]q^2 - C_\alpha q^{2\alpha-d}$ if $\alpha > \alpha_{\mathrm{cr}}$ [38], with $C_\alpha = -\kappa\pi^{(d/2)} 2^{d-2\alpha}\Gamma[(d/2)-\alpha]/\Gamma(\alpha)$. The expression of C_α depends on the boundary conditions: here we have assumed translational invariance. Inserting these expressions into Eq. (8), the characteristic function finally reads

$$K(\boldsymbol{q},t) \underset{q\to 0}{\simeq} \begin{cases} e^{-C_\alpha q^{2\alpha-d} t} & \alpha \leq \alpha_{\mathrm{cr}} \\ e^{-D_\alpha q^2 t} e^{-C_\alpha q^{2\alpha-d} t} & \alpha > \alpha_{\mathrm{cr}}. \end{cases} \tag{9}$$

For $\alpha \leq \alpha_{\mathrm{cr}}$, this is the characteristic function of a Lévy stable distribution [29–32], which is characterized by a long-range algebraic tail. Such a distribution corresponds to large but infrequent steps, the so-called rare events or big jumps relevant to a large variety of phenomena including motion of cold atoms in laser cooling, transport in turbulent flow, and neural transmission [49]. For $\alpha > \alpha_{\mathrm{cr}}$, instead, the

characteristic function has a peculiar mixed nature: it is the product of a Gaussian and of the Lévy flight factor.

From the inverse Fourier transform of $K(\boldsymbol{q}, t)$ we obtain the population $n_{\boldsymbol{j}}(t)$. For $\alpha \leq \alpha_{\rm cr}$ the asymptotic behavior $n_{\boldsymbol{j}}(t)$ depends on $\boldsymbol{j}$ as

$$n_{\boldsymbol{j}}(t) \underset{|\boldsymbol{j}|\gg 1}{\simeq} \kappa t/|\boldsymbol{j}|^{2\alpha}, \tag{10a}$$

while for $\alpha > \alpha_{\rm cr}$ we obtain the following mixed Gaussian and power-law behavior with increasing $|\boldsymbol{j}|$:

$$n_{\boldsymbol{j}}(t) \simeq \begin{cases} \frac{\exp(-|\boldsymbol{j}|^2/4D_\alpha t)}{(4\pi D_\alpha t)^{d/2}} & |\boldsymbol{j}| \lesssim \xi_{\alpha,t} \\ \kappa t/|\boldsymbol{j}|^{2\alpha} & |\boldsymbol{j}| \gg \xi_{\alpha,t}, \end{cases} \tag{10b}$$

which is one of the main results of this work. In Eq. (10b), $\xi_{\alpha,t}$ is the length scale at which the behavior crosses over from Gaussian to power law. For large enough time, $\xi_{\alpha,t}$ is well approximated by $\xi_{\alpha,t} \approx \sqrt{4D_\alpha t \log[4\alpha^\alpha \pi^{-d/2}\kappa^{-1} D_\alpha (4D_\alpha t)^{\alpha-\alpha_{\rm cr}}]}$ [38]. The exact expression of $\xi_{\alpha,t}$ exhibits a minimum as a function of α, and a discontinuity at $\alpha = \alpha_{\rm cr}$ [Fig. 1(a)]. For large α, $\xi_{\alpha,t}$ increases with α as $\xi_{\alpha,t} \sim \sqrt{4D_\alpha t \alpha \log \alpha}$, and we ultimately recover a standard diffusive (Gaussian) behavior for $\alpha \to \infty$. For $\alpha \to \alpha_{\rm cr}^+$, D_α diverges and therefore $\xi_{\alpha,t}$ does too. For small enough time, the power-law behavior takes over for all α. We emphasize that since $\xi_{\alpha,t}$ grows with time, the Gaussian dynamics ultimately dominates at long times for $\alpha > \alpha_{\rm cr}$, and thus we expect the algebraic tail to particularly affect transient phenomena.

This behavior is illustrated in Figs. 1(c) and 1(d) for $d = 1$, where we show a numerical solution of the CME [Eq. (7)] together with the asymptotic behavior Eq. (10). For $\alpha < \alpha_{\rm cr}$, the distribution is only characterized by a power-law decay with amplitude growing linearly with time and independent of the lattice dimension d [Fig. 1(c)]. The scaling with the distance $1/|\boldsymbol{j}|^{2\alpha}$ turns out to be the same as the hopping rate. While the decay of the distribution still goes as $\sim 1/|\boldsymbol{j}|^{2\alpha}$ at long distances for $\alpha > \alpha_{\rm cr}$, diffusion dominates at short distances showing a Gaussian profile [Fig. 1(d)], but with an enhanced diffusion coefficient D_α as compared to the nearest-neighbor case (inset). In the usual dipolar coupling case $\alpha = d = 3$, for instance, we find that D_α is enhanced by a factor ≈ 2.8 as compared to standard diffusion with nearest-neighbor hopping. Interestingly, we find that those power-law tails have a profound effect on the dynamics in the presence of strong dephasing for all α, which is surprising for $\alpha > \alpha_{\rm cr}$ where a simple diffusive behavior is expected from short-range models [14]. In the following, we illustrate this effect for the case of many excitons following a quench.

Many excitons: Speedup of relaxation.—We consider the dynamics in the many-exciton sector of Eq. (5) on a $d = 1$ lattice, starting from a "domain-wall" initial condition, where the leftmost $N/2$ sites are all occupied, while the other sites are empty, in analogy with a Joule expansion. We analyze the occupation profile at time t, i.e., $n_j(t) = \mathrm{Tr}[\rho(t) S_j^+ S_j^-]$, where $\rho(t)$ is the density matrix solving Eq. (5). Both for $\alpha < \alpha_{\rm cr}$ and for $\alpha > \alpha_{\rm cr}$, a flat equilibrium solution is reached at large t [38], such that $\bar{n} = \lim_{t\to\infty} n_j(t) = 0.5 \ \forall \ j$. Interestingly here, the equilibrium is reached for any hopping range α, which is in contrast to the purely quantum case, where long-range interactions can break ergodicity in the absence of disorder [50–52].

For short time $\kappa t \ll N^{2\alpha}$, the distribution away from the origin is dominated by single exciton hopping events, and we find that the profile has power-law tails [38]

$$n_j(t) \propto \kappa t \int_{-N/2}^{0} (j+r)^{-2\alpha} dr \approx \kappa t / j^{2\alpha-1}, \tag{11}$$

as shown in Fig. 2(a). As a consequence, the exciton spreads faster as α is decreased. To quantify how fast the equilibrium profile is reached, we compute the normalized chi-squared $\chi^2(t)/N = \sum_j [n_j(t) - \bar{n}]^2/(N\bar{n})$ between the profile at time t and the equilibrium one. Figure 2(b) shows that the equilibrium regime is reached exponentially in time for any α, $\chi^2(t)/N \propto \exp(-t/\tau)$. Note that this scaling can be recovered by analyzing the gap of the Liouvillian, Eq. (5), which follows from the spinon dispersion of the ferromagnetic Heisenberg model [53]. We observe that the half-time of the exponential increases with a power of the system size N as

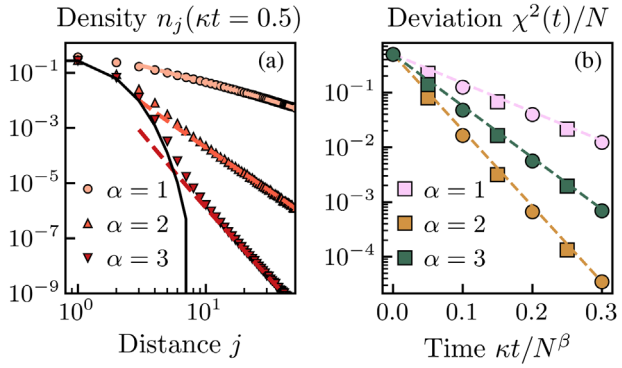

FIG. 2. Speedup of the relaxation dynamics for $d = 1$. Starting from a domain-wall exciton profile, the occupation profile $n_j(t)$ is computed numerically from Eq. (5) for $N = 100$ and $\kappa t = 0.5$ (a), and exhibits power-law tails showing that equilibrium is reached faster as α is decreased. The continuous line corresponds to nearest-neighbor hopping, and the dashed lines to the approximate solution Eq. (11). (b) Time evolution of the deviation from equilibrium $\chi^2(t)$ for different α and N. The circles and squares are for $N = 100$ and $N = 1000$, respectively. The dashed lines are the best fit $\propto \exp(-t/\tau)$, with τ given by Eq. (12).

$$\tau = \frac{N^\beta}{2\pi^\beta b_\alpha} \quad \text{with} \quad \beta = \begin{cases} 2\alpha - 1 & \alpha < \alpha_{\rm cr} \\ 2 & \alpha > \alpha_{\rm cr} \end{cases}, \tag{12}$$

for some constant b_α, while $\tau = (N^2 \log N/2\pi^2 b_\alpha)$ in the critical case $\alpha = \alpha_{\rm cr} = 3/2$. Notice that the scaling [Eq. (12)] is precisely what is expected from the continuous diffusion equation with (fractional) Laplacian,

$$\frac{\partial n(x,t)}{\partial t} = b_\alpha \Delta^{\beta/2} n(x,t). \tag{13}$$

Indeed, the solution to this evolution equation with an initial domain-wall density profile has the Fourier decomposition $n(x,t) = \frac{1}{2} + \sum_{m\in\mathbb{N}} c_m(t)\cos(\pi m x/N)$ with coefficients decaying as $c_m(t) \propto \exp(-b_\alpha(m\pi/N)^\beta t)$, thus $\chi^2(t) \propto N[n(x,t) - 1/2]^2 \propto \exp(-2\pi^\beta b_\alpha t/N^\beta)$.

The fact that the large-scale evolution of our system should be captured by a continuous diffusion equation with fractional Laplacian [Eq. (13)] follows from the form of the generator of the CME [Eq. (6)], which is SU(2) symmetric. Indeed, exploiting the SU(2) symmetry, one can switch from one "magnetization sector" to another, i.e., from one exciton number to another, without changing its spectrum. This suggests that the equation governing the evolution of the density profile for many excitons at large scales should be the same as for a single exciton. In particular, the constant b_α in Eq. (12) is expected to match the diffusion constant of a single exciton, i.e., $b_\alpha = D_\alpha$ for $\alpha > \alpha_{\rm cr}$ and $b_\alpha = C_\alpha$ for $\alpha < \alpha_{\rm cr}$. From the data in Fig. 2, we find the numerical values $b_\alpha/\kappa \simeq 1.93, 1.62, 1.1$ for $\alpha = 1, 2, 3$, to be compared with the analytical result $C_1/\kappa = 3.14$, $D_2/\kappa = 1.64$, $D_3/\kappa = 1.08$. The agreement is very good for $\alpha > \alpha_{\rm cr}$; however, the values differ in the long-range case $\alpha < \alpha_{\rm cr}$. This discrepancy is due to the different boundary conditions between the numerics in Fig. 2 (open boundary conditions) and in the analytical derivation of C_α (which assumes translational invariance, i.e., periodic boundary conditions). We also emphasize that β decreases with α for $\alpha < \alpha_{\rm cr}$, which implies that the equilibrium is reached faster (for large N) as the interaction range increases.

Outlook.—Our results provide a way to experimentally realize an exclusion process with long jumps [33–35], and are highly relevant to nanocrystal quantum dots that are attracting more and more interest for solar cell applications [20]. In particular, discrepancies between the exciton diffusion length measured experimentally and the values predicted by standard diffusion theory applied to Förster energy transfer ($\alpha = 3$) have been recently reported [15,39]. We argue in the Supplemental Material [38] that such discrepancies would typically be reduced by a factor of ~2 upon properly including the long-range character of the hopping in the diffusion coefficient, which is not the case in standard diffusion models assuming nearest-neighbor hopping [8]. Our model is also relevant to molecular aggregates that play an important role in photosynthetic complexes and optoelectronic devices [54]. Dye monomers interacting via dipole-dipole coupling ($\alpha = 3$) can indeed form highly ordered assemblies [55]. Supramolecular chemistry offers the possibility to control the mutual arrangement of monomers to achieve a nearest-neighbor hopping $J < 3$ THz, while the typical dephasing rate can exceed 14 THz at room temperature [18,19]. Our model could also be realized with ions in linear Paul traps, with $J \approx 100$–1000 Hz and the possibility to tune the hopping range within $0 < \alpha < 3$ [23,56,57]. Controlled dephasing can be realized via detuned lasers that induce time-dependent ac-Stark shifts [58], allowing to reach the large dephasing regime with $\gamma > 10J$ [27]. A similar implementation could also be achieved with Rydberg atoms [59], where the $\gamma \gg J$ regime can be reached for large atom densities.

We thank Shannon Whitlock, Johannes Schachenmayer, and Philipp Hauke for stimulating discussions. Numerical code for this work has been written in JULIA [60] and PYTHON, using QUANTUMOPTICS.JL [61] for the quantum master equation simulations. A. G. C. acknowledges support from the MOQS ITN programme, a European Union Horizon 2020 research and innovation program under the Marie Skłodowska-Curie grant agreement no. 955479. F. F. acknowledges support from the Croatian Science Funds Project No. IP-2019–4–3321 and the QuantiXLie Center of Excellence, a project cofinanced by the Croatian Government and European 12 Union through the European Regional Development Fund—the Competitiveness and Cohesion Operational Programme (Grant No. KK.01.1.1.01.0004). F. M. and G. P. acknowledge funding from the French ANR via project CLIMAQS. Computing time was provided by the High-Performance Computing Center of the University of Strasbourg.

[1] G. D. Scholes, Annu. Rev. Phys. Chem. **54**, 57 (2003).
[2] K. Feron, W. J. Belcher, C. J. Fell, and P. C. Dastoor, Int. J. Mol. Sci. **13**, 17019 (2012).
[3] S. M. Menke and R. J. Holmes, Energy Environ. Sci. **7**, 499 (2014).
[4] F. Fassioli, R. Dinshaw, P. C. Arpin, and G. D. Scholes, J. R. Soc. Interface **11**, 20130901 (2014).
[5] P. W. Anderson, Phys. Rev. **109**, 1492 (1958).
[6] B. Kramer and A. MacKinnon, Rep. Prog. Phys. **56**, 1469 (1993).
[7] F. Evers and A. D. Mirlin, Rev. Mod. Phys. **80**, 1355 (2008).
[8] O. V. Mikhnenko, P. W. M. Blom, and T.-Q. Nguyen, Energy Environ. Sci. **8**, 1867 (2015).
[9] S. Mukamel, Chem. Phys. **31**, 327 (1978).
[10] V. M. Kenkre and P. Reineker, *Exciton Dynamics in Molecular Crystals and Aggregates*, Springer Tracts in Modern Physics (Springer-Verlag, Berlin, Heidelberg, 1982).

[11] H. Haken and G. Strobl, Z. Phys. A-Hadron Nucl. **262**, 135 (1973).
[12] A. Madhukar and W. Post, Phys. Rev. Lett. **40**, 70 (1978).
[13] J. M. Moix, M. Khasin, and J. Cao, New J. Phys. **15**, 085010 (2013).
[14] M. V. Medvedyeva, F. H. L. Essler, and T. Prosen, Phys. Rev. Lett. **117**, 137202 (2016).
[15] A. J. Mork, M. C. Weidman, F. Prins, and W. A. Tisdale, J. Phys. Chem. C **118**, 13920 (2014).
[16] K. F. Chou and A. M. Dennis, Sensors **15**, 13288 (2015).
[17] E. Penzo, A. Loiudice, E. S. Barnard, N. J. Borys, M. J. Jurow, M. Lorenzon, I. Rajzbaum, E. K. Wong, Y. Liu, A. M. Schwartzberg, S. Cabrini, S. Whitelam, R. Buonsanti, and A. Weber-Bargioni, ACS Nano **14**, 6999 (2020).
[18] A. G. Dijkstra, H.-G. Duan, J. Knoester, K. A. Nelson, and J. Cao, J. Chem. Phys. **144**, 134310 (2016).
[19] T. Brixner, R. Hildner, J. Köhler, C. Lambert, and F. Würthner, Adv. Energy Mater. **7**, 1700236 (2017).
[20] M. A. Becker, L. Scarpelli, G. Nedelcu, G. Rainò, F. Masia, P. Borri, T. Stöferle, M. V. Kovalenko, W. Langbein, and R. F. Mahrt, Nano Lett. **18**, 7546 (2018).
[21] S. Davidson, F. A. Pollock, and E. Gauger, PRX Quantum **3**, 020354 (2022).
[22] P. Richerme, Z.-X. Gong, A. Lee, C. Senko, J. Smith, M. Foss-Feig, S. Michalakis, A. V. Gorshkov, and C. Monroe, Nature (London) **511**, 198 (2014).
[23] P. Jurcevic, B. P. Lanyon, P. Hauke, C. Hempel, P. Zoller, R. Blatt, and C. F. Roos, Nature (London) **511**, 202 (2014).
[24] J. Zeiher, J.-y. Choi, A. Rubio-Abadal, T. Pohl, R. van Bijnen, I. Bloch, and C. Gross, Phys. Rev. X **7**, 041063 (2017).
[25] S. de Léséleuc, V. Lienhard, P. Scholl, D. Barredo, S. Weber, N. Lang, H. P. Büchler, T. Lahaye, and A. Browaeys, Science **365**, 775 (2019).
[26] N. Defenu, T. Donner, T. Macrì, G. Pagano, S. Ruffo, and A. Trombettoni, Rev. Mod. Phys. (to be published).
[27] C. Maier, T. Brydges, P. Jurcevic, N. Trautmann, C. Hempel, B. P. Lanyon, P. Hauke, R. Blatt, and C. F. Roos, Phys. Rev. Lett. **122**, 050501 (2019).
[28] E. Valdinoci, arXiv:0901.3261.
[29] A. A. Dubkov, B. Spagnolo, and V. V. Uchaikin, Int. J. Bifurcation Chaos Appl. Sci. Eng. **18**, 2649 (2008).
[30] R. Metzler, A. V. Chechkin, V. Y. Gonchar, and J. Klafter, Chaos Solit. Fractals **34**, 129 (2007).
[31] V. Zolotarev, V. Uchaikin, and V. Saenko, J. Exp. Theor. Phys. **88**, 780 (1999).
[32] S. Janson, arXiv:1112.0220.
[33] M. D. Jara, Commun. Pure Appl. Math. **62**, 198 (2009).
[34] M. Jara, arXiv:0805.1326.
[35] C. Bernardin, P. Cardoso, P. Goncalves, and S. Scotta, arXiv:2007.01621.
[36] H.-P. Breuer, F. Petruccione *et al.*, *The Theory of Open Quantum Systems* (Oxford University Press on Demand, New York, 2002).
[37] H. Pichler, A. J. Daley, and P. Zoller, Phys. Rev. A **82**, 063605 (2010).
[38] See Supplemental Material at http://link.aps.org/supplemental/10.1103/PhysRevLett.131.053401 for plots of the exciton density profile for $d > 1$, an alternative derivation of the CME [Eq. (7)], the full derivation of $\langle \boldsymbol{j}(t) \rangle$ and $\langle |\boldsymbol{j}|^2(t) \rangle$, α_{cr}, $\mathcal{A}_{2\alpha,d}(\boldsymbol{q})$, $n_j(t)$, $\xi_{\alpha,t}$, Eq. (6), the many-exciton $n_j(t)$, as well as a treatment of the weak dephasing regime, which includes Refs. [10,15,38–41].
[39] D. Giovanni, M. Righetto, Q. Zhang, J. W. M. Lim, S. Ramesh, and T. C. Sum, Light Sci. Appl. **10**, 2 (2021).
[40] F. Olver, D. Lozier, R. Boisvert, and C. Clark, *The NIST Handbook of Mathematical Functions* (Cambridge University Press, New York, NY, 2010).
[41] V. Eisler, J. Stat. Mech. (2011) P06007.
[42] Z. Cai and T. Barthel, Phys. Rev. Lett. **111**, 150403 (2013).
[43] D. Bernard, T. Jin, and O. Shpielberg, Europhys. Lett. **121**, 60006 (2018).
[44] J.-S. Bernier, P. Barmettler, D. Poletti, and C. Kollath, Phys. Rev. A **87**, 063608 (2013).
[45] D. Poletti, P. Barmettler, A. Georges, and C. Kollath, Phys. Rev. Lett. **111**, 195301 (2013).
[46] J. J. García-Ripoll, S. Dürr, N. Syassen, D. M. Bauer, M. Lettner, G. Rempe, and J. I. Cirac, New J. Phys. **11**, 013053 (2009).
[47] D. Rossini, A. Ghermaoui, M. B. Aguilera, R. Vatré, R. Bouganne, J. Beugnon, F. Gerbier, and L. Mazza, Phys. Rev. A **103**, L060201 (2021).
[48] F. D. M. Haldane, Phys. Rev. Lett. **60**, 635 (1988); B. S. Shastry, Phys. Rev. Lett. **60**, 639 (1988).
[49] A. Vezzani, E. Barkai, and R. Burioni, Sci. Rep. **10**, 2732 (2020).
[50] H. Korbmacher, P. Sierant, W. Li, X. Deng, J. Zakrzewski, and L. Santos, Phys. Rev. A **107**, 013301 (2023).
[51] W.-H. Li, X. Deng, and L. Santos, Phys. Rev. Lett. **127**, 260601 (2021).
[52] E. Khatami, G. Pupillo, M. Srednicki, and M. Rigol, Phys. Rev. Lett. **111**, 050403 (2013).
[53] H. Nakano and M. Takahashi, Phys. Rev. B **50**, 10331 (1994).
[54] F. Würthner, T. E. Kaiser, and C. R. Saha-Möller, Angew. Chem. Int. Ed. **50**, 3376 (2011).
[55] N. J. Hestand and F. C. Spano, Chem. Rev. **118**, 7069 (2018).
[56] C. Monroe, W. C. Campbell, L.-M. Duan, Z.-X. Gong, A. V. Gorshkov, P. W. Hess, R. Islam, K. Kim, N. M. Linke, G. Pagano, P. Richerme, C. Senko, and N. Y. Yao, Rev. Mod. Phys. **93**, 025001 (2021).
[57] I. Pogorelov, T. Feldker, C. D. Marciniak, L. Postler, G. Jacob, O. Krieglsteiner, V. Podlesnic, M. Meth, V. Negnevitsky, M. Stadler, B. Höfer, C. Wächter, K. Lakhmanskiy, R. Blatt, P. Schindler, and T. Monz, PRX Quantum **2**, 020343 (2021).
[58] N. Trautmann and P. Hauke, Phys. Rev. A **97**, 023606 (2018).
[59] H. Schempp, G. Günter, S. Wüster, M. Weidemüller, and S. Whitlock, Phys. Rev. Lett. **115**, 093002 (2015).
[60] J. Bezanson, A. Edelman, S. Karpinski, and V. B. Shah, SIAM Rev. **59**, 65 (2017).
[61] S. Krämer, D. Plankensteiner, L. Ostermann, and H. Ritsch, Comput. Phys. Commun. **227**, 109 (2018).